

High Sensitivity CMOS-MEMS Relative Humidity Sensor Based on Electrothermal Actuation

A. Y. Ahmed¹, G. Witjaksono¹, J. O. Dennis², M. H. Md Khir¹, Almur. A. S. Rabih¹, Muhammad. U. Mian¹ and Mawahib. G. A. Ahmed¹

¹Department of Electrical and Electronic Engineering, Universiti Teknologi PETRONAS, 32610 Bandar Seri Iskandar, Perak Darul Ridzuan, Malaysia.

²Department of Fundamental and Applied Sciences, Universiti Teknologi PETRONAS, 32610 Bandar Seri Iskandar, Perak Darul Ridzuan, Malaysia.

johndennis@utp.edu.my

Abstract—This paper presents a high sensitivity CMOS-MEMS humidity sensor based on electrothermal actuation for application in indoor relative humidity monitoring. The detection is based on the principle of amplitude change as a result of absorption/adsorption or desorption of the humidity molecules onto the surface of a titanium dioxide (TiO₂) active material deposited on a moving plate of the sensor resulting into a change of its mass. The CMOS-MEMS humidity sensor measurement is performed after preconditioning in which the sensor goes through early actuation before the real measurement is done. The sensor is operated in the dynamic mode at an actuation input frequency of 2 Hz and a driving voltage varied from 2 V_{pp} to 6 V_{pp}. The maximum output voltage observed was at 4 Hz, which is double the input frequency. The voltage was found to increase linearly from 8.728 mV to 71.117 mV with the increase in driving voltage from 2 V_{pp} to 6 V_{pp}. The response of the device to humidity shows linear output voltage change from 66.998 mV to 69.822 mV when relative humidity increases from 40% RH to 60% RH with a sensitivity of 0.14 mV/% RH.

Index Terms—CMOS-MEMS; Humidity sensing; Electrothermal; Titanium dioxide.

I. INTRODUCTION

Humidity is the amount of water vapor in a mixture of gases like air or pure gas such as nitrogen or argon. Monitoring and measurement of humidity are very crucial in many areas such as agriculture, automated systems, instrumentation, climatology, etc. [1]. Moreover, humidity also affects the human comfort [2], as the comfortable indoor relative humidity for the occupants was reported to be between 35% RH and 65% RH [3]. Humidity can be expressed or measured in different forms and relative humidity (RH) is the most used form. RH is a temperature dependent parameter, defined as the ratio of the partial pressure of the water vapor to the saturation pressure of the gas that the water vapor is mixed to at the given temperature.

Several microstructures with a sensitive layer or material coating have been used as humidity sensors. These sensors operate at room temperature; hence they suffer from desorption of the humidity once absorbed causing irregularities in the detection process. Complementary Metal Oxide Semiconductor Microelectromechanical System (CMOS-MEMS) is an example of microstructures sensor. There are two fundamentally different operation modes: (a) static mode [4] and (b) dynamic mode [5]. To operate the sensor in the dynamic mode, energy supplied to the device is

converted to a mechanical motion. There are several ways to convert the supplied energy into mechanical forms, such as electrostatic [6-8], piezoelectric [9-12], electromagnetic [13, 14] and electrothermal [15-22].

The principle of electrothermal actuation of the micro-machined sensor is based on temperature variations. These variations in temperature affect the sensors in two ways [23]: (1) dimension of the sensor changes or stress developed inside the device, (2) material properties of the device change as a function of temperature. Electrothermal actuation has been used in several applications due to many advantages such as high force, lower actuation voltages, ease of implementation in the device and CMOS compatible fabrication. This technique relies on heating of the embedded resistances (heating elements) in MEMS devices by applying AC-current through them. This method will generate motion with displacement due to thermal expansion of the materials.

Many types of electrothermal actuation have been reported and studied; Hot/cold arm [24-26], bi-material or bimorph [25, 27] and thermal buckling actuator [25, 28]. Figure 1 shows an example of schematics of types of electrothermal actuation microactuators design: (a) hot/cold arm (b) bi-material, (c) V-shaped beams (buckling actuators) and (d) shuttle beams (buckling actuators).

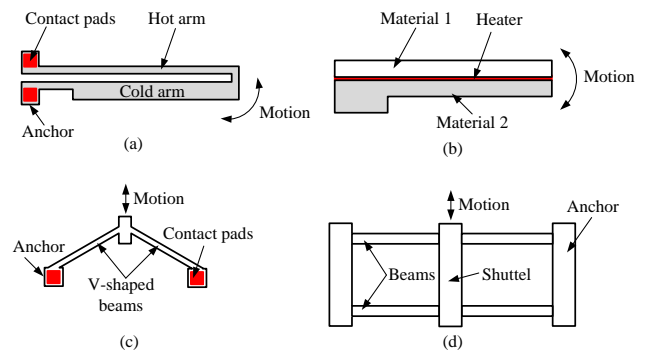


Figure 1: Schematics of electrothermal actuators (a) hot and cold arm, (b) bi-material and buckling actuator, (c) V-shaped beams and (d) shuttle beams

In the hot and cold arm, the actuator is made of a hot arm (narrow), a cold arm (wide) flexure anchor and pads. When a voltage difference is applied across the contact pads, the current is passed through, and the hot arm (higher resistance) heats up more than the cold arm (lower resistance) due to larger current density in the narrower hot arm. The difference

in the thermal expansion between the two arms causes the hot arm temperature to increase, which will produce expansion in one material more than the other resulting in thermal stresses and bending the device.

The bi-material actuator consists of two or more layers of different materials bonded together. When the current is applied, the temperature of the bi-material is raised. This temperature will produce expansion in one material more than the other resulting in thermal stresses and bending the device. The thermal buckling actuator consists of V-shaped beams or shuttle beams, anchors and contact pads. When current is passed through it, the thermal expansion due to Joule heating induces thermal expansion moving the shuttle or pushing the central beam of the device forward.

The objective of this paper is to improve the sensitivity of CMOS-MEMS humidity sensor by preconditioning before taking its measurement.

II. CMOS-MEMS DEVICE DESIGN AND FABRICATION

Figure 2 shows a schematic design and dimensions of various components of the device. The CMOS-MEMS device consists of a single released plate hanging by the support of four beams. The support beams are based on two sections of the same length but different widths. The designed CMOS-MEMS sensor has two sensing mechanisms, piezoresistive using PZR elements and capacitive using comb fingers. For the reported study, only the PZR sensing mechanism was used. The schematic cross-sectional view of the device viewed along AA' is shown in Figure 3.

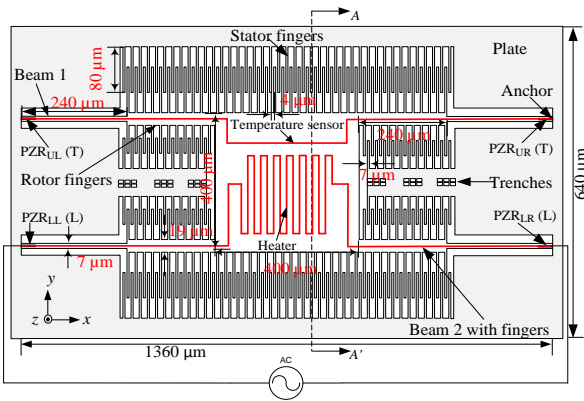


Figure 2: Schematic design and dimensions of the resonator

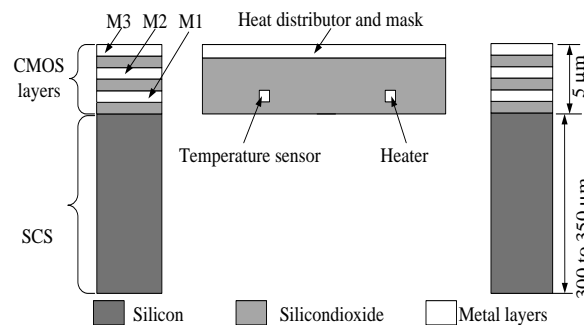


Figure 3: Cross-sectional view along AA' showing CMOS layers and the SCS substrate

The sensor was developed by fabricating the MEMS device using standard 0.35 μm CMOS process technology and then followed by a post-CMOS micromachining process. The

CMOS process consists of two polysilicon, three metal, several dielectric layers and two vias. All metal layers are aluminium, whereas silicon dioxide (SiO₂) is used as the dielectric layer and tungsten is used for the vias.

CMOS-MEMS humidity sensor is actuated electrothermally by passing a sinusoidal (AC) current through an embedded microheater. The AC current produces a temperature in the plate, and this temperature is translated into mechanical force due to the difference of coefficient of thermal expansion. The generated force makes the sensor to resonate in the dynamic mode following the frequency of the AC current, out of a plane in the z-axis. The stress produced at the anchor of the supporting beams is measured through resistance change of the embedded piezoresistive (PZR) elements, by arranging them in Wheatstone bridge circuit configuration for a stable output. The electrothermal generated power is given by Equation (1) [29-31].

$$P(t) = \frac{V_{ac}^2}{R} = \frac{A^2 \cos^2(\omega t)}{R} = \frac{A^2}{2R} + \frac{A^2}{2R} \cos(2\omega t) \quad (1)$$

where R is the electrical resistance of the microheater. The generated heat (thermal power) consists of static component $A^2/2R$ and dynamic component $A^2/2R \cos(2\omega t)$. Equation (1) indicates that the frequency of the generated power is double the input frequency.

The mathematical modeling, simulation, fabrication and deposition of TiO₂ sensitive layer of the CMOS-MEMS device has been presented in our previously published research [32-35]. Figure 4 shows a Field Emission Scanning Electron Microscope (FESEM) image of the TiO₂ material deposited on the moving plate of the CMOS-MEMS device.

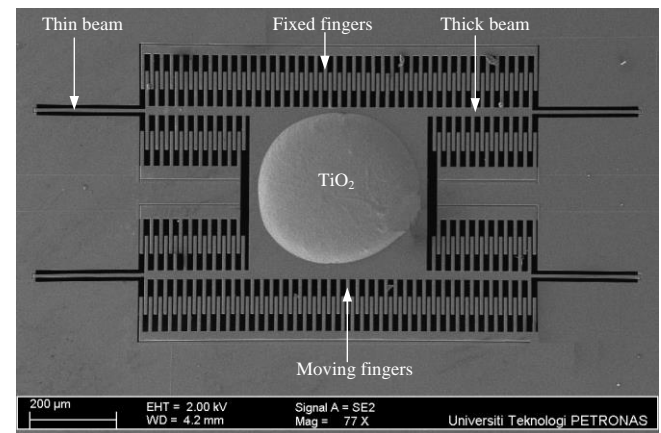


Figure 4: FESEM image of TiO₂ paste deposited on the moving plate of the CMOS-MEMS humidity sensor

III. CHARACTERIZATION SETUP

The CMOS-MEMS device consists of four PZR for sensing purpose. The setup is constructed using one PZR of the device connected to three external resistors R_1 , R_2 and R_3 of the same values to form Wheatstone quarter bridge configuration. The bridge is biased using 3 V DC, and the output is fed into instrumentation amplifier with the gain of 200. The amplified signal is connected to SR 770 FFT network analyzer as shown in Figure 5.

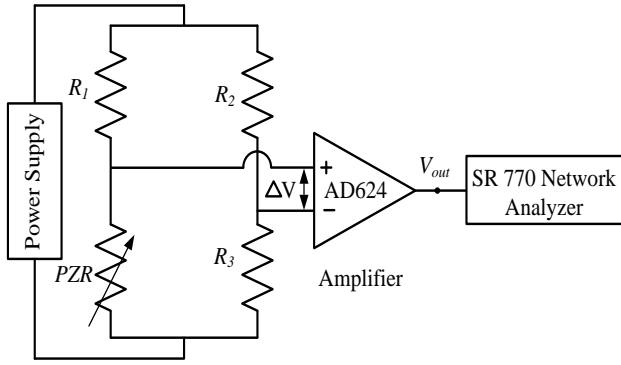


Figure 5: Wheatstone bridge with amplifier for measurement of output sensing signal of piezoresistive and three external resistors R_1 , R_2 and R_3

The CMOS-MEMS sensor is driven in the dynamic mode at a lower frequency than the intended frequency to preconditioning the MEMS device so that it will perform at optimum condition during operation. In this operation, the initial frequency is set to be 0.5 Hz lower than the optimum frequency of 2 Hz and the reading will be taken at that optimum frequency. The sensor is driven using voltage from $2 V_{pp}$ to $6 V_{pp}$ at 2 Hz. Schematic diagram of the experimental setup is shown in Figure 6 for the characterization of the of the CMOS-MEMS device for the relative humidity response. The system consists of a tank of dry air connected to the test chamber through two paths. Valve (2) is allocated in the first path while the second path is connected by the valve (3) that allows dry air to pass through water container and valve (4). The flow of the dry air is controlled by the valve (1) and flow meter. For the calibration, a standard humidity and temperature sensor (model HT-601C) is placed inside the chamber to measure and verify the temperature and humidity inside the chamber.

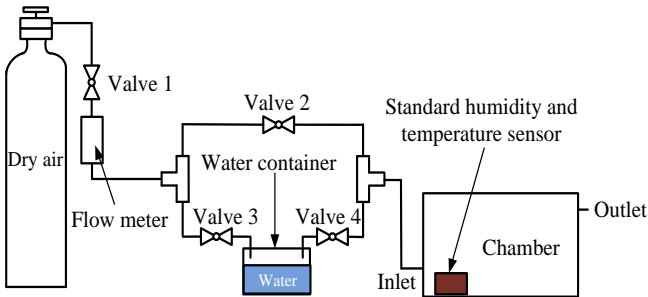


Figure 6: Schematic of the experimental setup for chamber calibration

Prior to the introduction of humidity into the test chamber, one liter/min of dry air was flowed through the test chamber using the first path via the valve (2) to reduce the humidity inside the chamber from ambient humidity of about 75% RH to 37% RH. Once the minimum humidity of 37% RH is achieved, the humidity inside the chamber can be increased by flowing the dry air through the second path over water surface in the container. To calibrate the chamber, the humidity was varied from 38% to 62% RH in steps of 5% RH and the standard humidity sensor (model HT-601C) was used to record the humidity.

The calibration of the test chamber for the humidity levels and temperature leads to the device characterization where the CMOS-MEMS device was placed inside the chamber on a specially designed sample holder as shown in figure 7. The device is operated in dynamic mode at 2 Hz input frequency

and $6 V_{pp}$ (corresponding to an operating temperature of 80°C as determined from Temperature Coefficient of Resistance (TCR) measurements [36]).

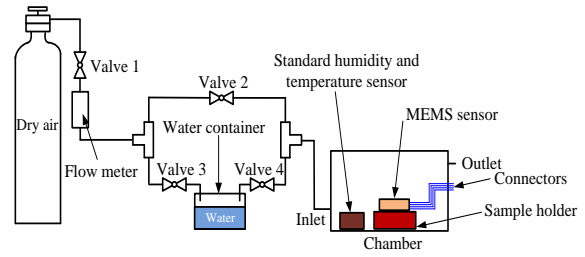


Figure 7: Schematic of the experimental setup for characterization of the relative humidity response of the CMOS-MEMS device

IV. RESULTS AND DISCUSSION

Figure 8 shows the maximum output voltage as a function of the driving voltage at 2 Hz input frequency. It can be seen that the output voltage increases linearly from 8.728 mV to 71.117 mV with increasing the driving voltage from $2 V_{pp}$ to $6 V_{pp}$. The increase in the driving voltage has a proportional stress effect at the anchor of the supporting beams resulting in an increase of the resistance of the piezoresistive (PZR) element, which will, in turn, produce a linear change in the output voltage. An example of the output voltage of the CMOS-MEMS device form SR 770 FFT network analyzer is shown in Figure 9. This output voltage was obtained by applying $3 V_{pp}$ driving voltage at an input frequency of 2 Hz.

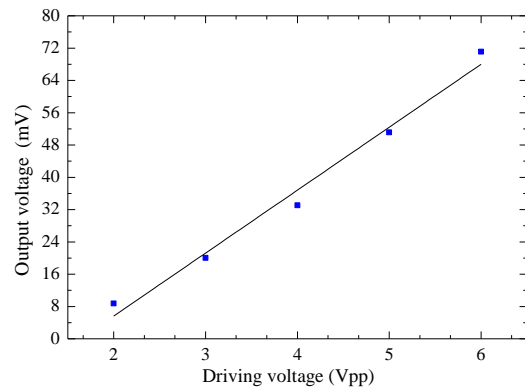


Figure 8: Graph of the maximum output voltage vs. driving voltage from $2 V_{pp}$ to $6 V_{pp}$ at input frequency of 2 Hz

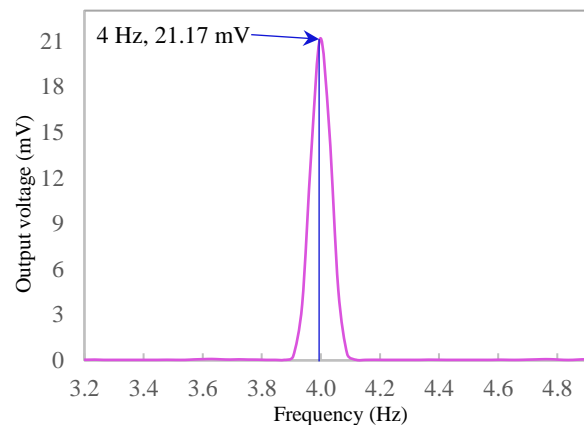


Figure 9: Output spectrum of the CMOS-MEMS device at double frequency of 4 Hz

To calibrate the chamber, standard humidity and temperature sensor (model HT-601C) is used to measure relative humidity and the temperature inside the chamber as a function of time for the humidity increase from 38% RH to 62% RH. Figure 10 shows the relationship between the humidity and the time as linear, while Figure. 11 indicates a constant chamber temperature of 24.9 °C.

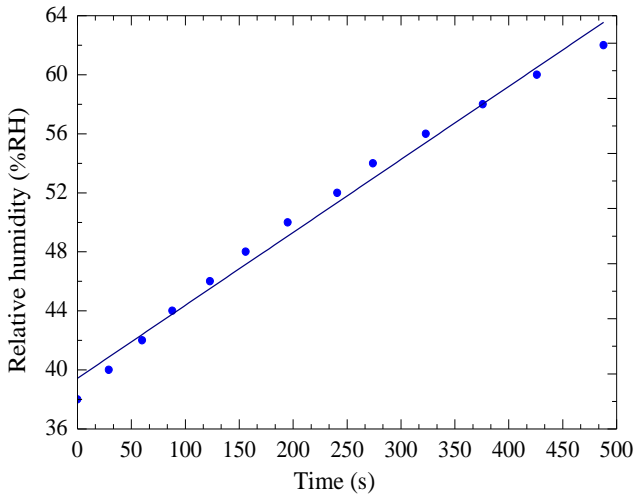


Figure 10: Linear rise in relative humidity (from 38% RH to 62% RH) vs. time as dry air flows over water in container (chamber calibration)

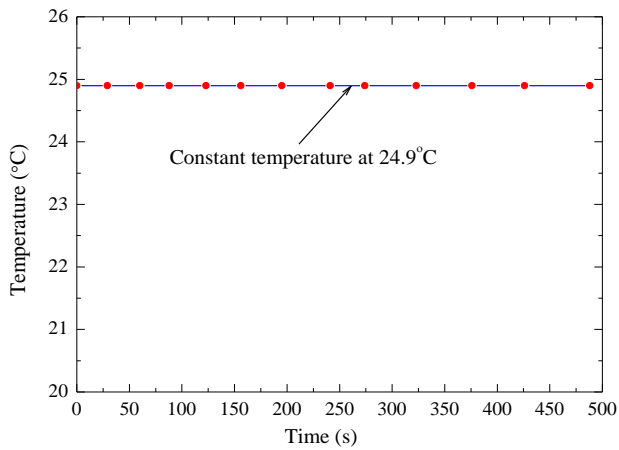


Figure 11: Temperature measurement inside chamber vs. time as the humidity is varied from 38% RH to 62% RH (chamber calibration)

Figure 12 shows experimental results of the output spectrum of the CMOS-MEMS humidity sensor when the relative humidity varies from 40% RH to 60% RH. The device is operated in dynamic mode at an optimum frequency of 2 Hz and 6 V_{pp} (corresponding to an operating temperature of 80 °C as determined from TCR measurements [36]). J. O. Dennis et al. [35] presented a humidity sensor having linear increments in the sensitivity from temperature 40 °C to 80 °C. The sensitivity increase with the temperature is the expected result of is due to the desorption effect of gaseous species such as H₂O in humidity detection on the TiO₂ surface. The desorption effect is enhanced with an increase in temperature resulting in an increase in sensitivity because of desorption of gaseous species such as H₂O in the MEMS sensor increases. With the increase in temperatures, higher amount of vaporous species desorb from the sensor surface (TiO₂), bringing about a general reduction in the mass of the plate and causing an increase in the amplitude of the vibrating structure.

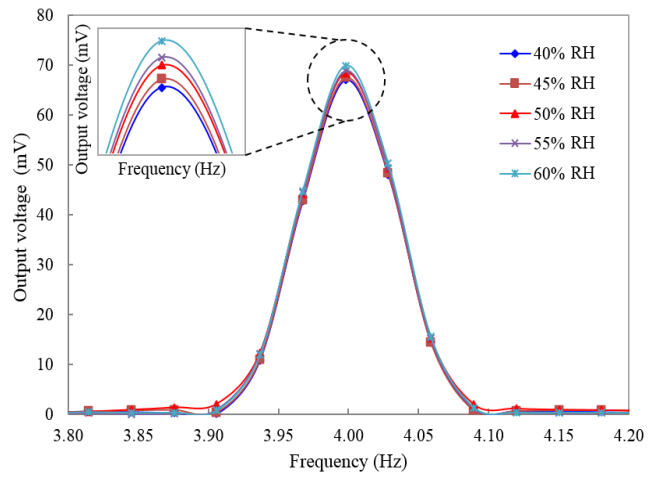


Figure 12: Output spectrum of the CMOS-MEMS device vs. changes in relative humidity level from 40% RH to 60% RH

It is observed that after preconditioning in which initial frequency is added before the measurement the maximum output voltage of the device increases linearly from 66.998 mV to 69.822 mV with an increase in the relative humidity level from 40% RH to 60% RH as shown in Figure 13. The sensitivity of the CMOS-MEMS device is found to be 0.14 mV/% RH. This efficiency is 30% higher than the results being reported before [35].

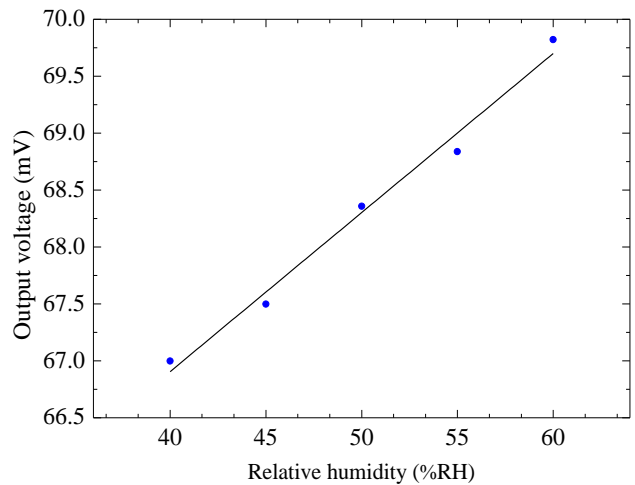


Figure 13: Output voltage at 2 Hz 6 V_{pp} driving voltage vs. relative humidity (operating temperature of 80 °C)

V. CONCLUSION

A CMOS-MEMS humidity sensor is electrothermally actuated at a frequency of 2 Hz and applying different driving voltages (2 V_{pp} to 6 V_{pp}). After the preconditioning, the output voltage is found to increase linearly with increasing the driving voltage. The chamber is calibrated against humidity and showed a linear rise in relative humidity as a function of time. The output voltage of the device increases linearly from 66.998 mV to 69.822 mV with an increase in the relative humidity level from 40% RH to 60% RH. The sensitivity of the device is found to be 0.14 mV/% RH which is 30% higher than the value reported before 0.107 mV/% RH.

ACKNOWLEDGMENT

The authors would like to thank Universiti Teknologi PETRONAS (UTP) for funding this research under Short-Term Internal Research Fund (STIRF) cost center number: 0153AA-F63.

REFERENCES

- [1] H. Farahani, R. Wagiran, and M. Hamidon, "Humidity Sensors Principle, Mechanism, and Fabrication Technologies: A Comprehensive Review," *Sensors*, vol. 14, p. 7881, 2014.
- [2] K. S. Choi, D. S. Kim, H. J. Yang, M. S. Ryu, J. S. Chae, and S. P. Chang, "Comparison and analysis of capacitive humidity sensors with water vapor inlet holes of different depths," *Journal of Micro/Nanolithography, MEMS, and MOEMS*, vol. 14, 2015.
- [3] R. Fenner and E. Zdankiewicz, "Micromachined water vapor sensors: a review of sensing technologies," *Sensors Journal, IEEE*, vol. 1, pp. 309-317, 2001.
- [4] J. Fritz, M. K. Baller, H. P. Lang, H. Rothuizen, P. Vettiger, E. Meyer, H. -J. Güntherodt, C. Gerber, and J. K. Gimzewski, "Translating Biomolecular Recognition into Nanomechanics," *Science*, vol. 288, pp. 316-318, 2000.
- [5] A. Hierlemann, and H. Baltesa "CMOS-based chemical microsensors," *Analyst*, vol. 128, pp. 15-28, 2003.
- [6] B. Mukherjee, K. B. M. Swamy, and S. Sen, "A new approach for sensitivity improvement of MEMS capacitive accelerometer using electrostatic actuation," in *Sixth International Conference on Sensing Technology (ICST)*, 2012, pp. 738-742.
- [7] I. Voiculescu, M. E. Zaghoul, Fellow, IEEE, R. A. McGill, E. J. Houser, and G. K. Fedder, "Electrostatically actuated resonant microcantilever beam in CMOS technology for the detection of chemical weapons," *Sensors Journal, IEEE*, vol. 5, pp. 641-647, 2005.
- [8] S. S. Bedair, and G. K. Fedder, "CMOS MEMS Oscillator for Gas Chemical Detection," in *Sensors. Proceedings of IEEE*, 2004, pp. 955-958.
- [9] R. Nuryadi, A. Djajadi, R. Adiel, L. Aprilia and N. Aisah, "Resonance Frequency Change in Microcantilever-Based Sensor due to Humidity Variation," *Materials Science Forum*, vol. 737, pp. 176-182, 2013.
- [10] L. Khine, J. M. Tsai, A. Heidari, and Y. Yong-Jin, "Piezoelectric MEMS resonant gas sensor for defence applications," in *Defense Science Research Conference and Expo (DSR)*, 2011, pp. 1-3.
- [11] G. Uma, M. Umapathy, L. B. Vidhya, M. Maya, T. Sophia, and K. Tamarasi, "Design and analysis of resonant based gas sensor," in *Sensors Applications Symposium SAS 2008 IEEE*, pp. 119-121.
- [12] V. A. Thakar, Z. Wu, A. Peczalski, and M. Rais-Zadeh, "Piezoelectrically Transduced Temperature-Compensated Flexural-Mode Silicon Resonators," *Journal of Microelectromechanical Systems*, vol. 22, pp. 815-823, 2013.
- [13] V. Berouille, Y. Bertrand, L. Latorre, and P. Nouet, "Monolithic piezoresistive CMOS magnetic field sensors," *Sensors and Actuators A: Physical*, vol. 103, pp. 23-32, 2003.
- [14] A. L. H. May, P. J. G. Ramírez, L. A. A. Cortés, E. Figueras, J. M. Castillo, E. Manjarrez, A. Saucedo, L. G. González, and R. J. Aguirre, "Mechanical design and characterization of a resonant magnetic field microsensor with linear response and high resolution," *Sensors and Actuators A: Physical*, vol. 165, pp. 399-409, 2011.
- [15] A. Hajjam and S. Pourkamali, "Fabrication and Characterization of MEMS-Based Resonant Organic Gas Sensors," *Sensors Journal, IEEE*, vol. 12, pp. 1958-1964, 2012.
- [16] A. Hajjam, A. Logan, and S. Pourkamali, "Fabrication and characterization of MEMS-based resonant organic gas sniffers," in *Sensors, IEEE*, 2011, pp. 1105-1108.
- [17] A. Rahafrooz and S. Pourkamali, "Fully micromechanical piezo-thermal oscillators," in *2010 IEEE International Electron Devices Meeting (IEDM)*, 2010, pp. 7.2.1-7.2.4.
- [18] A. Hajjam, J. Pandiyan, A. Rahafrooz, and S. Pourkamali, "MEMS resonant sensors for detection of gasoline vapor," in *Sensors, IEEE*, 2010, pp. 1538-1541.
- [19] J. C. W. Arash Hajjam1, Amir Rahafrooz1 and Siavash Pourkamali1, "Fabrication and characterization of thermally actuated micromechanical resonators for airborne particle mass sensing: II. Device fabrication and characterization," *Journal of Micromechanics and Microengineering*, vol. 20, 2010.
- [20] A. Rahafrooz and S. Pourkamali, "High-Frequency Thermally Actuated Electromechanical Resonators with Piezoresistive Readout," *IEEE Transactions on Electron Devices*, vol. 58, pp. 1205-1214, 2011.
- [21] A. Rahafrooz, A. Hajjam, B. Tousifar, and S. Pourkamali, "Thermal actuation, a suitable mechanism for high frequency electromechanical resonators," in *IEEE 23rd International Conference on Micro Electro Mechanical Systems (MEMS)*, 2010, pp. 200-203.
- [22] A. Hajjam, A. Logan, J. Pandiyan, and S. Pourkamali, "High frequency thermal-piezoresistive MEMS resonators for detection of organic gases," in *Joint Conference of the IEEE International Frequency Control and the European Frequency and Time Forum (FCS)*, 2011, pp. 1-5.
- [23] B. Bahreyni, *Fabrication & Design of Resonant Microdevices: Elsevier Science*, 2008.
- [24] V. Kumar and N. Sharma, "Design and Validation of Silicon-on-Insulator Based U Shaped Thermal Microactuator," *International Journal of Materials, Mechanics and Manufacturing*, vol. 2, pp. 86-91, 2014.
- [25] N. Islam, *Microelectromechanical Systems and Devices. Janeza Trdine 9, 51000 Rijeka, Croatia InTech*, 2012.
- [26] A. Kalaiarasi and S. HosiminThilagar, "Design and Finite Element Analysis of Electrothermal Compliant Microactuators," in *Proceedings of Bangalore Conference*, 2011.
- [27] H. Sehr, I. Tomlin, B. Huang, S. Beeby, A. Evans, A. Brunnschweiler, G. Ensell, C. Schabmueller, and T. Niblock, "Time constant and lateral resonances of thermal vertical bimorph actuators," *Journal of Micromechanics and Microengineering*, vol. 12, p. 410, 2002.
- [28] E. T. Enikov, S. S. Kedar, and K. V. Lazarov, "Analytical model for analysis and design of V-shaped thermal microactuators," *Journal of Microelectromechanical Systems*, vol. 14, pp. 788-798, 2005.
- [29] T. S. J. Lammerink, M. Elwenspoek, R. H. Van Ouwwerkerk, S. Bouwstra, and J. H. J. Fluitman, "Performance of thermally excited resonators," *Sensors and Actuators A: Physical*, vol. 21, pp. 352-356, 1990.
- [30] T. S. J. Lammerink, M. Elwenspoek, and J. H. J. Fluitman, "Frequency dependence of thermal excitation of micromechanical resonators," *Sensors and Actuators A: Physical*, vol. 27, pp. 685-689, 1991.
- [31] O. Brand, H. Baltes, and U. Baldenweg, "Thermally excited silicon oxide beam and bridge resonators in CMOS technology," *IEEE Transactions on Electron Devices*, vol. 40, pp. 1745-1753, 1993.
- [32] J. O. Dennis, A. Y. Ahmed, M.H.M Khir and A. A. S. Rabih, "Modelling and Simulation of the Effect of Air Damping on the Frequency and Quality factor of a CMOS-MEMS Resonator" *Applied Mathematics and Information Sciences. (AMIS) 2015*, 9, 729-737.
- [33] A. Y. Ahmed, J. O. Dennis, M. H. Md Khir, M. N. Mohamad Saad and M. R. Buyong, "Design, Simulation and Fabrication of a Mass Sensitive CMOS-MEMS Resonator," *Sensors & Transducers Journal*, vol. 17, pp. 40-49, 2012.
- [34] A. Y. Ahmed, J. O. Dennis, M. H. Md Khir and M. N. Mohamad Saad, "Deposition of titanium dioxide nanoparticles on the membrane of a CMOS-MEMS resonator", *AIP Conference Proceedings, 3rd International Conference on Fundamental and Applied Sciences (ICFAS 2014)*, V 1621, N 1, pp 522-529.
- [35] J. O. Dennis, A. Y. Ahmed and M. H. Md Khir, "Fabrication and Characterization of a CMOS-MEMS Humidity Sensor", *Sensors 2015*, vol. 15, pp. 16674-16687.
- [36] A. Y. Ahmed, J. O. Dennis, M. H. M. Khir and M. N. M. Saad, "Design and Characterization of Embedded Microheater on CMOS-MEMS Resonator for Application in Mass-Sensitive Gas Sensors". In *Proceedings of the 2014 5th International Conference on Intelligent and Advanced Systems: Technological Convergence for Sustainable Future (ICIAS)*, Kuala Lumpur, Malaysia, 3-5 June 2014; pp. 1-4.